IVYSPRING INTERNATIONAL PUBLISHER

Theranostics

2013; 3(9):667-676. doi: 10.7150/thno.6650

Review

Necrosis Avidity: A Newly Discovered Feature of Hypericin and its Preclinical Applications in Necrosis Imaging

Binghu Jiang[1], Jichen Wang[1], Yicheng Ni[2], Feng Chen[1, 2]✉

1. Department of Radiology, BenQ Medical Center, Nanjing Medical University, Nanjing 210019, China.
2. Theragnostic laboratory, Department of Imaging and Pathology, University Hospital, University of Leuven, 3000 Leuven, Belgium.

✉ Corresponding author: Feng Chen, MD, PhD. Department of Radiology, BenQ Medical Center, Nanjing Medical University, Nanjing 210019, China. Or Theragnostic laboratory, Department of Imaging and Pathology, University Hospital, University of Leuven, Herestraat 49, Bus 7003, 3000 Leuven, Belgium. Telephone: +32-16-330165 Fax: +32-16-343765 E-mail: chenfengbe@yahoo.com.cn.

Received: 2013.05.08; Accepted: 2013.07.06; Published: 2013.08.10

Abstract

Hypericin has been widely studied as a potent photosensitizer for photodynamic therapy in both preclinical and clinical settings. Recently, hypericin has also been discovered to have a specific avidity for necrotic tissue. This affinity is also observed in a series of radiolabeled derivatives of hypericin, including [^{123}I]iodohypericin, [^{124}I]iodohypericin, and [^{131}I]iodohypericin. Hypericin, along with other necrosis-avid contrast agents, has been investigated for use in noninvasively targeting necrotic tissues in numerous disorders. Potential clinical applications of hypericin include the identification of acute myocardial infarction, evaluation of tissue viability, assessment of therapeutic responses to treatments, and interventional procedures for solid tumors. The mechanisms of necrosis avidity in hypericin remain to be fully elucidated, although several hypotheses have been suggested. In particular, it has been proposed that the necrosis avidity of hypericin is compound specific; for instance, cholesterol, phosphatidylserine, or phosphatidylethanolamine components in the phospholipid bilayer of cellular membranes may be the major targets for its observed selectivity. Further investigations are needed to identify the specific binding moiety that is responsible for the necrosis avidity of hypericin.

Key words: hypericin, necrosis, avidity

Introduction

The polycyclic aromatic molecule hypericin is a naturally occurring chromophore extracted from *Hypericum perforatum*, the plant commonly known as St. John's wort [1] (Fig. 1). Hypericin easily forms aggregates and sparingly dissolves in few solvents. When dissolved in certain organic solvents, it consistently exhibits well-resolved spectral bands with absorption maxima around 540 and 590 nm, and red fluorescence emission maxima around 590 and 640 nm. Interest in hypericin has grown following the discovery that it possesses high photocytotoxic towards tumors and certain viruses, including human immunodeficiency virus. This toxicity requires excitation via external light [2]. Since the absorption maxima of hypericin are at longer wavelengths, excitation light can reach hypericin in deeper tumors. Importantly, hypericin is also highly photostable, with its fluorescence detectable for up to 16 hours after instillation. This photostability can be further enhanced by formulation with 40% N-methyl pyrrolidone (NMP) [3]. Over recent decades, hypericin has been actively studied in photodynamic therapy as a

potent photosensitizer due to its high triplet quantum and singlet oxygen yield, and other reactive oxygen species (ROS) that are associated with photo-oxidative cellular damage. Its photocytotoxic action has been explored in a variety of experimental and clinical settings, including cancer detection, and therapeutic activities toward tumors [1, 4-6], viruses [7], bacteria [8] , and fungi [9]. It was recently discovered that hypericin has a peculiar affinity for necrotic tissues [10-18], independent of its photosensitivity. Several radiolabeled derivatives of hypericin, such as [^{123}I]iodohypericin [19-24] and [^{131}I]iodohypericin [25], have shown similar necrotic affinity in a number of pathological processes, including in animal models with organ infarctions or tumor necrosis. Thus, hypericin has also been recognized as a necrosis-avid contrast agent (NACA) [10, 18, 19], and is a focus of interest in relation to necrosis imaging. Due to their high sensitivity and specificity toward necrotic tissues, NACAs have been used as specific magnetic resonance imaging (MRI) markers for noninvasive targeting of tissue necrosis in numerous disorders [19-24, 26-32]. Application of NACAs include acute myocardial infarction identification [16, 28, 33], tissue viability evaluation [27, 30-32], assessment of therapeutic responses to drug treatment [14], and interventional procedures [26] in subjects with solid tumors.

The promising results reported to date suggest potential clinical uses of NACAs. Therefore, the significant value of hypericin as an NACA merits further exploration. In this mini-review, we focus on the necrosis-targeting characteristic of hypericin.

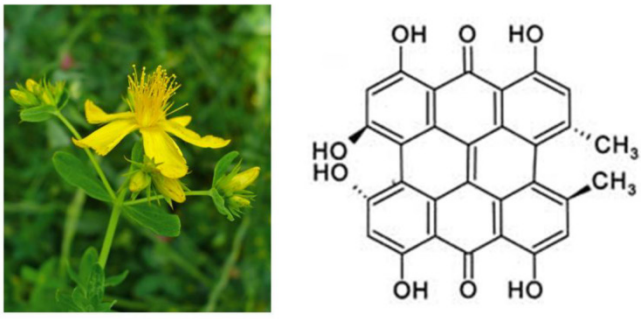

Fig 1. (A) Photograph of St. John's wort. (B) Chemical structure of hypericin.

Necrosis-avid contrast agents (NACAs)

As the finding of necrosis avidity in hypericin is tightly linked with the discovery of NACAs, it is necessary to briefly introduce some background information about NACAs. Additional details about NACAs can be found in a review by Ni et al. [10].

Discovery of NACAs as MR imaging markers

As early as 1924, it was reported that porphyrins selectively accumulate in tumor tissues [34]. Consequently, people took advantage of this characteristic of porphyrins for tumor localization and photosensitization for photodynamic therapy [35]. Since the early 1980s, paramagnetic metalloporphyrins—mainly Bis-Gd-DTPA-mesoporphyrin (Gadophrin-2), Bis-Gd-DTPA-mesoporphyrin-Cu (Gadophrin-3), and Mn-tetraphenylporphyrin (Mn-TPP)—have been developed as promising tumor-specific MRI contrast agents for use in tumor-seeking studies [36, 37]. Animal experiments have shown that intravenous or intraperitoneal injections of metalloporphyrins may exhibit delayed "tumor-specific" enhancements [36].

However, the results of several studies by Ni et al. [30, 31, 33] challenge the concept of tumor-specific retention of porphyrin derivatives. For example, animal experiments revealed specific metalloporphyrin accumulation in acute myocardial infarction [33]. Additionally, in a liver tumor animal model, contrast-enhanced MR imaging with two porphyrin-based contrast agents (Gadophrin-2 and Mn-TPP) showed that the sustained contrast-enhanced area represented pathologically necrotic and non-viable tissues, rather than viable neoplastic tissues [30]. Subsequent experiments on liver tumor models consistently confirmed that the reportedly tumor-specific contrast enhancement was solely localized to the necrotic tumor components [14, 26]. To further validate these findings, Ni et al. [31], [38] tested more metalloporphyrins in various animal models of benign necrosis, including bile-obstructive hepatic infarction, alcohol-induced liver necrosis, reperfusion liver lobe infarction, segmental renal infarction, and acute myocardial infarction. The results showed that the necrosis-specific accumulation of metalloporphyrins could be reproduced in both benign and tumoral necrosis, and the peak enhancement was about 24 hours after metalloporphyrin administration [31]. Based on those findings, Ni et al. [10, 18] proposed the concept of NACAs to describe porphyrin derivatives that selectively accumulate in necrotic tissues and can be used as MRI contrast agents.

Thus, there exists a discrepancy between the tumor-specific and necrosis-specific features of porphyrins derivatives. There are several possible explanations for this inconsistency. First, in some studies, the "tumor-specific" evidence of porphyrin was represented by combined enhancements in both the tumor and necrotic areas, without associated patho-

logical data; therefore, it could not be separated and evaluated whether the porphyrin retention was located in the viable or necrotic tumor parts [36, 39-42]. Additionally, while the metalloporphyrins were found to have an affinity for neoplastic tissues, substantial extra-tumoral concentrations were also noted. This was likely because both the viable and necrotic tumor tissues were enhanced with porphyrin derivatives [43, 44]. Secondly, there are technical variations between studies. For instance, one study presented only non-specific enhancement in the early phase after porphyrin injection, which was not sufficient to demonstrate tumor specificity [34]. Third, porphyrin derivatives may vary in their accumulation mechanisms, and thus their properties of water solubility, tumor or necrosis affinity, and paramagnetic features could be remarkably affected by even minor modification of the derivative structure [45, 46].

Despite this controversy regarding tumor specificity, all results have demonstrated selective accumulation of metalloporphyrins in necrotic tissues (malignant or benign necrosis), regardless of the sites and causes of necrotic tissues. Furthermore, numerous studies from different groups [47-49] confirmed the discoveries reported by Ni et al. Overall, the data explicitly identify the real targets of these paramagnetic porphyrin-based contrast agents as necrotic tissues, despite the non-specific enhancement of other intact organs and tissues, including viable tumor parts. Consequently, these porphyrin-based compounds—and the later developed non-porphyrin species, namely Bis-Gd-DTPA-pamoic acid derivative (ECIII-60) and Bis-Gd-DTPA-bis-indole derivative (ECIV-7)—were termed necrosis-avid contrast agents [10]. These research efforts have led to a shift from metalloporphyrin use as "tumor-seeking" contrast agents to their use as markers of nonviable tissues [28]. Over time, the necrosis avidity of NACAs has gradually been validated in the biomedical imaging community [50, 51].

Functional features of NACAs

Novel applications of NACAs for preclinical experiments in cardiovascular, oncological, and molecular imaging research continue to emerge [32, 51, 52]]. All studied NACAs, whether porphyrin or non-porphyrin species, allow differential diagnoses between necrotic tissue and viable tissue. Even negative findings showing no contrast enhancement 24 hours after intravenous NACA injection can help to reliably exclude the presence of necrosis and reaffirm tissue viability, which would be very useful for differential diagnosis [53]. Another promising application was recently presented for NACAs in therapeutic assessment after interventional procedures, like radiofrequency ablation (RFA) of malignant tumors to differentiate residual tumor tissue from peri-ablation benign reactive tissues [26]. It was demonstrated that with the gradual wash-out of non-specific liver contrast enhancement, complete tumor ablation was indicated with a specific rim or "O" type contrast enhancement around the RFA lesion at 24 hours after NACA administration, while incomplete tumor ablation resulted in an incomplete rim or "C" type enhancement with moderately discernible contrast at the residual viable tumor [17] (Fig. 2). Their discrimination of necrotic tissue from living tissue is one advantage of NACAs over other contrast agents for this particular application. NACAs also share some features commonly seen in other types of contrast agents; for instance, their relatively long plasma half-life resulting from protein binding facilitates their utility as blood-pool contrast agents for MR angiography [10]. Overall, NACAs exhibit combined specific and non-specific capacities, and may serve well as versatile MR imaging contrast agents [18].

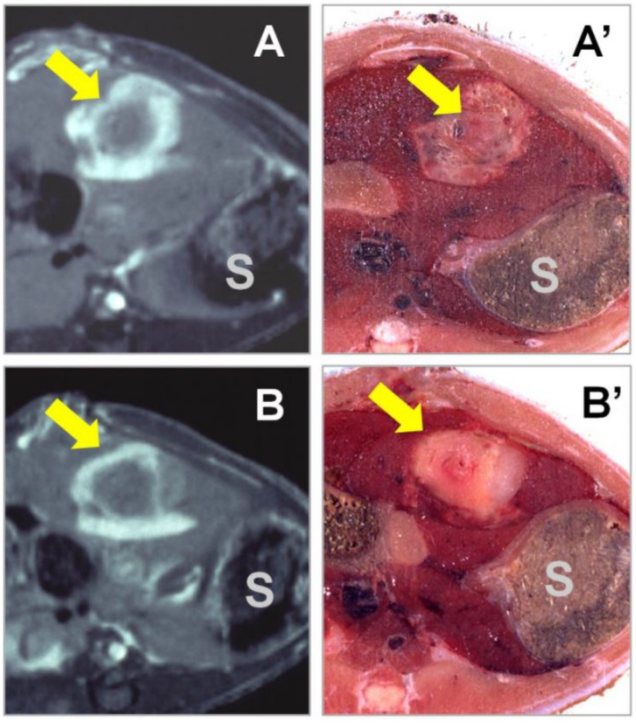

Fig 2. T1-weighted contrast-enhanced MR images were acquired 24 hours after i.v. injection of the nonporphyrin necrosis-avid contrast agent bis-Gd-DTPA-bis-indole derivative (ECIV-7) at 0.05 mmol/kg in rats with liver implantation of rhabdomyosarcoma (arrow) treated with RFA. "S" denotes the adjacent stomach. (A & A') The cross-sectional MR image and corresponding body slice in a rat with complete liver tumor ablation, clearly demonstrating an "O" type persistent contrast enhancement. (B & B') The cross-sectional MR image and corresponding body slice in a rat with incomplete liver tumor ablation, clearly demonstrating a "C" type persistent contrast enhancement. Figure modified from Ni Y et al. Eur Radiol 2006 16: 1031–1040 with permission.

Practically, it appears that NACAs exert the necrosis-targeting function only when denatured non-viable tissue debris is present in the living body. Otherwise, they behave like other non-specific contrast agents, e.g., the extracellular fluid contrast agents used for MR imaging. Indeed, studies have demonstrated multiple functional features of NACAs, including non-specific contrast enhancement soon after injection; the persistent blood-pool effect due to the 2.5-hour plasma half-life; and striking necrosis avidity at advanced stages, typically 24 hours after injection [10]. Experimentally, NACAs have been used as multifunctional MRI contrast agents in various settings, for instance, contrast enhancement MRI in abdomen solid organs, like liver and kidneys; MR angiography; first-pass myocardial MR perfusion and delayed enhanced MRI for myocardial viability assessment; and MRI monitoring and evaluation of tumor responses to therapies [10].

From NACAs to hypericin

In terms of necrosis imaging applications, there are currently three main types of NACAs. The first type is for ex vivo or postmortem use, and is hardly applicable for imaging or clinic applications. One such NACA is Evans blue, which has been used as a standard reference for visualizing myocardial [54] and cerebral infarctions [55] in pathological sections. The second type is used for MR imaging, and includes the above-mentioned porphyrin and non-porphyrin NACAs. The porphyrin derivatives have little potential for clinical use due to intrinsic defects [10]. The third type of NACA bears radionuclides for use in nuclear scintigraphy, such as radionuclide-labeled monoclonal antibodies (TNT MAb) for tumor necrosis treatment and radiolabeled annexin V (Table 1). Due to their superb sensitivity in targeting necrotic tissue, radionuclide-labeled NACAs have attracted much attention in the development of necrosis-specific molecular imaging markers.

As an emerging NACA, hypericin exhibits high necrosis avidity that can be visualized with macro- and microscopic fluorescence, and radiolabeled hypericin derivatives that share these necrosis-targeting characteristics can be prepared simply and inexpensively. In this manner, hypericin and its radiolabeled derivatives have expanded the spectrum of NACAs from single MRI markers to nuclear and optical tracers with highly increased sensitivity of necrosis detection [20, 22] (Table 1). Preclinical studies have so far demonstrated the utility of the necrotic-targeting feature of hypericin and its derivatives in three main kinds of necrotic models.

Table 1. Representative necrosis avid contrast agents.

Name	Generic name	Molecular target	MW (kDa)	Biological function	Source of imaging signal/contrast	Imaging technique
C34-H24-N6-Na4-O14-S4	Evans blue	Unknown	0.96	necrosis	Color, Flu	Flu, Mic, Mac
Bis-Gd-DTPA mesoporphyrin	Gadophrin-2 Gd-MP	Unknown	1.7	necrosis	Gd-	MRI
Bis-Gd-DTPA-Mesoporphyrin-Cu	Gadophrin-3	Unknown	1.8	necrosis	Gd-	MRI
Mn-tetraphenylporphyrin	Mn-TPP	Unknown	1.1	necrosis	Mn-	MRI
Bis-Gd-DTPA-pamoic acid derivative	ECIII-60	Unknown	1.6	necrosis	Gd-	MRI
Bis-Gd-DTPA-bis-Indole derivative	ECIV-7	Unknown	1.6	necrosis	Gd-	MRI
Annexin V		PS	36	apoptosis, necrosis	^{99m}Tc, ^{123}I, ^{111}In, ^{67}Ga, ^{18}F, ^{68}Ga	SPECT PET
C2A domain of synaptotagmin I		PS	12	apoptosis, necrosis	^{99m}Tc	SPECT
PSBP-6		PS	1.6	apoptosis, necrosis	^{99m}Tc	SPECT
Duramycin		PE	2	apoptosis, necrosis	^{99m}Tc	SPECT
Pyrophosphate		Unknown, Ca^{2+}?	0.25	necrosis	^{99m}Tc	SPECT
Antimyosin mAb	R11D10-FAb	heavy chain of intracellular myosin	50	necrosis	^{99m}Tc, ^{111}In	SPECT
Glucarate		histone proteins	0.21	necrosis	^{99m}Tc	SPECT
TNT MAb	TNT-1 TNT-3, chTNT	histone H1 and DNA single stranded DNA	25-55	necrosis	^{131}I, ^{125}I, ^{111}In	SPECT
Hypericin		cell membranes (PS, PE Cholesterol)? subcellular organelle	0.5	necrosis	^{99m}Tc, ^{125}I, ^{123}I, ^{131}I ^{64}Cu	SPECT PET

Flu: fluorescence; Mac: macroscope; Mic: microscope; MMW: molecular weight; PS: phosphatidylserine; PE: phosphatidylethanolamine; TNT MAb: tumor necrosis treatment monoclonal antibody; chTNT: chimeric TNT.

Organ ischemic necrosis

Ni et al. [20] conducted the pioneer work discovering the necrosis avidity of hypericin. Mono-[^{123}I]iodohypericin was evaluated with in vivo single-photon emission computed tomography (SPECT) imaging in animal models of infarctions in the liver of rat and the heart of rabbit. Both the hepatic and cardiac infarct areas showed well-defined hot spots that were persistently visualized over 48 hours. This accumulation of mono-[^{123}I]iodohypericin in necrotic tissue was perfectly consistent with the images from post-mortem triphenyltetrazolium chloride (TTC) staining, autoradiography (ARx), and histology. At 60 hours post-injection, the radioactivity concentration was over 10 times higher in liver infarct tissues (3.51% ID/g) than in normal liver tissues (0.38% ID/g), and over 6 times higher in heart infarct tissues (0.36% ID/g) than in normal myocardium (0.054% ID/g). On selected parts of ARX images, the radioactivity ratios of infarct to normal tissue were as high as 18 (Figs. 3, 4).

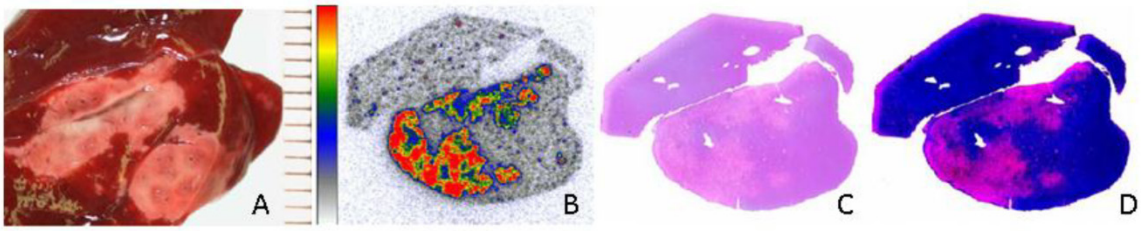

Fig 3. Necrotic accumulation of ^{123}I-hypericin in a rat liver lobe with focal reperfused infarction. (A) Triphenyltetrazolium chloride (TTC) staining of a liver lobe with focal reperfused infarction. The normal liver tissue (red) and necrotic tissue (pale) were sampled for radioactivity counting. (B-D) Analyses of the 50-μm frozen liver slice adjacent to the slice used for TTC in A. (B) Autoradiography results showing that the radioactivity of ^{123}I was high in necrotic tissue, and low in normal liver tissue. (C) Histological results with H&E staining. (D) H&E staining results with enhanced contrast and brightness. The necrotic area seen upon H&E staining in C and D was closely matched with the area with high radioactivity upon autoradiography in B. Figure modified from Ni Y et al. Eur J Nucl Med Mol 2006; 33: 595–601 with permission.

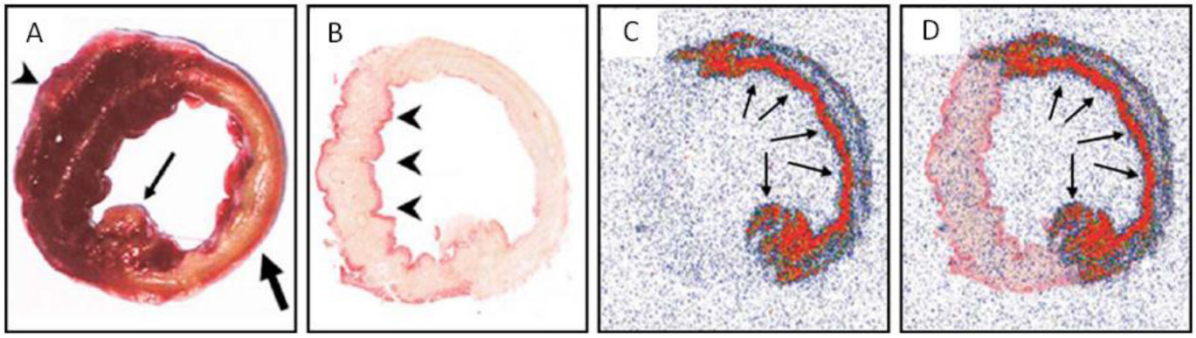

Fig 4. Necrotic accumulation of ^{123}I-hypericin on the ex vivo images of a rabbit heart with infarction. (A) A TTC-stained 5-mm-thick slice with right ventricular wall attached (arrowhead), showing the transmural infarction (pale) involving the entire anterior and lateral wall of the left ventricle (thick arrow), including the posterior papillary muscle (thin arrow). (B) A TTC-stained 50-μm frozen slice with the right ventricular wall removed, showing the non-infarcted myocardium (arrowheads) at the posterior wall and the interventricular septum (superficially stained brick red). (C) A 50-μm slice subjected to autoradiography, showing a "doughnut" pattern of radioactivity uptake that appears only in the infarcted region. The highest activity (in red) is found mainly subendocardially and near the lateral border zone, where the tracer can diffuse from the blood circulation into this occlusive myocardial infarct (arrows). (D) The overlapped the image of TTC staining (B) with the autoradiographic image (C) showed a perfect match of the high radioactivity area with the infarcted region (arrows). Figure reprinted from Ni Y et al. Eur J Nucl Med Mol 2006; 33: 595–601 with permission.

Therapeutic tumoral necrosis induced with minimally invasive procedures

In a murine model, Van de Putter et al. [11] studied hypericin as a potential imaging biomarker for early monitoring of therapeutic response after radiofrequency ablation (RFA) of liver tumors. Taking advantage of the compound's fluorescent property, they used a fluoromicroscope to show that the mean hypericin fluorescence density in necrosis was about 5 times and 12 times higher than in viable tumor and normal liver tissue, respectively. These results indicated a promising use of hypericin to differentiate between necrotic and viable tissues. In another study, murine liver tumor treated with chemical ablation using absolute ethanol showed preferential uptake of hypericin in ethanol-induced necrotic tissue, which was almost identical to that observed in RFA-induced necrotic tissues [13]. It has also been shown that the extent of hypericin accumulation in necrotic tissue depends on the time of administration. For instance, hypericin injection shortly (1 hour) before ablation is preferable to after ablation, because significant ex-

travasations occur during ablation, allowing greater hypericin access into the entire necrotic area. If the hypericin is injected 24 hours after ethanol treatment, it accumulates only at the peripheral region of necrosis, creating a fluorescent rim and leaving large areas without any hypericin deposit due to lack of access. It was found that the no-entry zones for hypericin, or large necrotic areas, mainly comprise dehydrated tissue with signs of severe cell damage and loss of tissue structure on H&E stains.

Use of necrotic zone abutting viable tumor as a target for radiolabeled hypericin, to deliver radiation devastation to adjacent viable tumor cells

Despite encouraging outcomes in treating solid tumors by inducing central tumor necrosis with anti-vasculature approaches, e.g., vascular disrupting agent, viable tumor residues frequently cause the eventual incomplete therapy and tumor relapse. To tackle this problem, the necrosis-avid property of hypericin was utilized to carry a tumoricidal substance, e.g., ^{131}I, to kill the abutting viable tumor. To proof this principle, Ni's group first used a vascular disrupting agent (combretastatin A4 phosphate; CA4P) to cause massive tumor necrosis in rat liver tumor models [25]. Then, iodine ^{131}-labeled hypericin (^{131}I-hypericin) was i.v. injected to reach and accumulate in the necrotic zone. The 131I-hypericin showed a remarkable necrotic avidity, with a target-to-liver ratio over 20. This dose was estimated almost 100 times the cumulative dose of 50 Gy that is necessary for effective radiotherapy. The ^{131}I-hypericin that accumulated in the necrotic zone destroyed the adjacent tumor cells with ionizing radiation, and significantly inhibited tumor regrowth (Fig. 5). A subsequent study by Van de Putte et al. [11] in nude mice bearing radiation-induced fibrosarcoma (RIF-1) further verified the radiotherapeutic effect of ^{131}I-hypericin, taking advantage of its necrotic avidity. FDG micro-PET results confirmed significantly delayed tumor growth compared to in the control group. The prolonged survival and simultaneous theranostic benefit of this approach is also demonstrated in a more recent animal study [56]. Considering that necrosis is a commonly seen feature of solid tumors following anticancer treatments, this dual-targeting approach using radiolabeled hypericin for both tumor diagnosis and therapy appears to have promising potential.

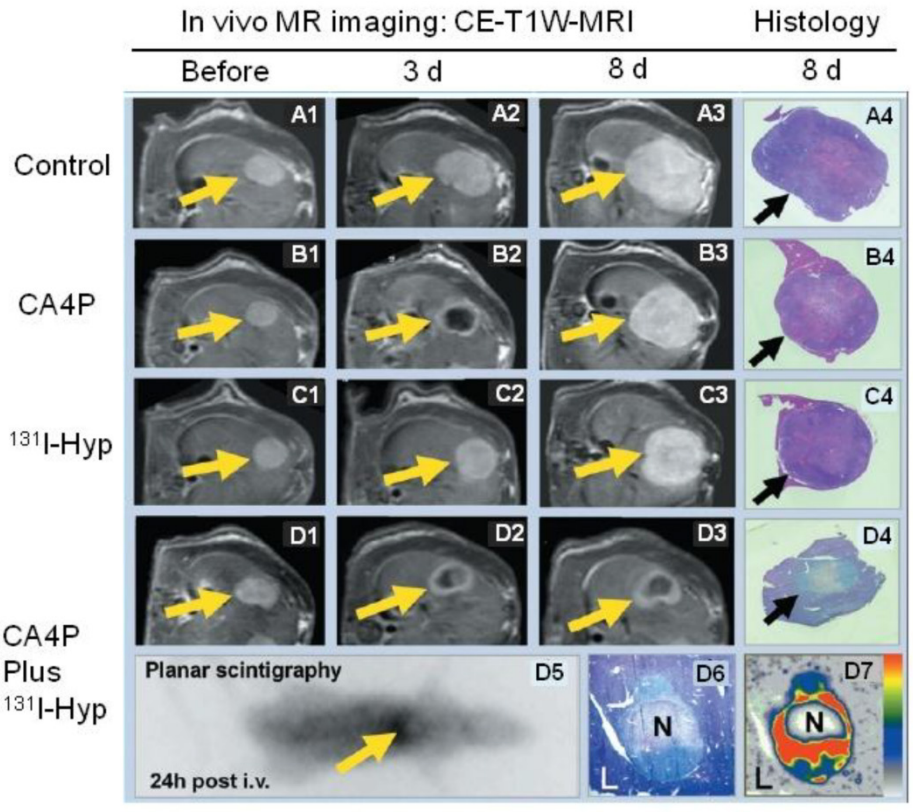

Fig 5. Representative results from a hypericin-mediated dual-targeting anticancer approach in four groups of rats. (A1-A4) Group A included control animals. Implanted liver rhabdomyosarcoma tumors (R1) grew rapidly during the entire experiment. (B1-B4) Group B was treated with the vascular targeting agent CA4P. B2 shows obvious vascular shutdown and necrosis seen as rim enhancement at three days after treatment, and B3 showed rapid tumor enlargement. (C1-C4) Group C was treated with ^{131}I-hypericin (^{131}I-Hyp), and tumor growth was only moderately inhibited. (D1-D7) Group D was treated with a combination of CA4P and ^{131}I-Hyp. The CA4P-induced necrosis was used as an initial target to lead ^{131}I-Hyp to deliver radiation devastation to the second target, the adjacent viable tumor cells. D2 and D3 show that the tumor virtually stopped growing, with a persistently unenhanced tumor center. D5 shows the planar gamma scintigraph evidence of radioactivity accumulation in the necrotic tumor, which was verified by colocalized histologic slide show in D6 and autoradiograph in D7. In vivo MRI findings were verified with histopathological analysis of H&E stained slides in terms of tumor dimensions and viability. H&E staining of tumor tissue appears paler on D4 and D6 than that of surrounding healthy liver (L). In contrast, the H&E staining of healthy liver in groups A, B, and C is paler than that of tumor tissue in A4, B4, and C4, suggesting viability at risk (reduced nucleus substance) due to constant regional ionizing radiation in group D. CE-T1W-MRI = contrast-enhanced T1-weighted magnetic resonance imaging; Hyp = hypericin; i.v. = intravenous therapy; N = necrotic tumor tissue. Figure modified from Li J et al. Radiology 2011; 260(3): 799-807 with permission.

The mechanism of necrosis avidity behind hypericin

The future development and application of hypericin necessitate a more complete knowledge of the necrosis-avidity mechanism. The mechanism of necrosis avidity in hypericin has not yet been fully elucidated, although several thoughts or hypotheses were raised to explain the phenomenon.

Necrosis avidity as a natural feature following necrosis

Necrosis is an accidental, passive, and unregulated form of cell death resulting from physiochemical damage and sudden metabolic failure. Necrotic cell death is typically associated with a loss of membrane integrity, release of cell contents, and inflammation induced by proteolytic enzymes and other cytosolic materials [57]. Following autolysis, the disintegrated cell membrane facilitates direct communication between necrotic debris and hypericin or other NACAs. Hypericin and other NACAs show a high affinity for necrotic tissues, independent of the cell type or cause of injury. Hypothetically, hypericin or NACAs may specifically bind to certain exposed sites of subcellular substances, such as degraded proteins, peptides, and nucleotides that are present in the necrotic tissue. Those binding sites are key points in the necrosis avidity to NACA-like molecules. Additionally, unlike the wash-out process of non-specific imaging contrast agents that occurs over a few minutes, the final clearance of hypericin and NACAs from necrotic tissue typically takes a few days after administration. This delayed clearance is probably reflective of the progressive infiltration and phagocytosis by inflammatory cells, resulting in the eventual removal of NACA together with necrotic debris, and replacement by granulation tissue [21, 40]. Following this hypothesis, the avidity of certain chemicals to necrotic debris and stromal molecules in the living body may be considered as an effect of the native autonomous wound healing process. However, this general assumption is insufficient to explain the specific mechanisms of necrosis avidity for NACA-like molecules [58].

Albumin-binding is required for necrosis avidity

Hofmann et al. [59] investigated the molecular mechanism by which the NACA gadophrin-2 targets necrotic tumor tissue. Based on fluorescence spectrophotometry results, the authors attributed the necrotic accumulation of gadophrin-2 to its binding to serum albumin or interstitial albumin, and not to other proteins, lipids, or DNA. However, in a model of reperfused liver infarction, Ni et al. [38] compared gadophrin-2 with the strong albumin-binding blood-pool contrast agent MP2269, and they observed necrosis-specific contrast enhancement with gadophrin-2 but not with MP-2269. This result suggested that albumin-binding is not a necessary condition for the necrotic avidity of NACAs, and that the role of albumin binding in the mechanisms of NACAs should be reevaluated [58].

Low-density lipoprotein (LDL) binding

In photodynamic therapy, photosensitizers are predominantly transported to various areas of the body with serum proteins. In general, highly hydrophobic photosensitizers like hypericin interact mainly with lipoproteins, especially low-density lipoproteins (LDL) [22, 60]. Van de Putter et al. [60] dynamically observed the uptake and retention of hypericin and DiOC18-labeled lipoproteins in necrotic subcutaneous tumors in mice. Based on both visual and quantitative fluorescence analysis, they reported no accumulation of labeled lipoproteins in necrosis at 24 hours after injection. Furthermore, the study showed a 50-100% difference in fluorescence intensities regarding the localization between hypericin and labeled lipoproteins. These results strongly suggested that the lipoprotein might serve as a vehicle only during hypericin transport, and that hypericin was released from the lipoprotein complex before reaching the necrotic tumor tissue [12, 60]. Several reports have confirmed that the LDL and LDL receptor pathway plays an important role in the delivery of hypericin into the cells [61-63].

Cholesterol binding in lipid membranes

Since the lipophilic property of hypericin should lead to its preferential localization in the lipid components of the cell membrane bilayer [64], it was suggested that hypericin transportation and accumulation are related to the properties and behaviors of membrane lipids. In a model of giant unilamellar vesicle membrane systems, Ho et al. [65] identified cholesterol (a major component in the surface lipids of LDL) as the major target for the observed selectivity of hypericin. Using phase-separated dipalmitoylphosphatidylcholine (DPPC)/cholesterol monolayer experiments, they found that hypericin effectively packs with cholesterol. As hypericin and cholesterol have the same molecular morphology of a rigid planar configuration, cholesterol may attract hypericin more competently than other lipids, which was demonstrated by emission spectrum spectroscopy and fluorescence microscopy of hypericin in lipid

monolayers.

Phospholipid binding in lipid membranes

In an animal study, Song et al. [66] labeled hypericin with ^{64}Cu in chelation with bis-DOTA to form ^{64}Cu-bis-DOTA-hypericin for PET imaging of necrosis. Therapeutic necrosis was induced with near-infrared photothermal ablation therapy in a breast xenograft tumor mouse model. PET imaging demonstrated increased ^{64}Cu-bis-DOTA-hypericin uptake in necrotic tissues at 24 hours after i.v. injection. Additionally, surface plasmon resonance experiments examining the selective avidity of bis-DOTA-hypericin to the main lipid components in the membrane bilayer structure showed higher selective avidity to phosphatidylserine (PS) and phosphatidylethanolamine (PE) compared to phosphatidylcholine (PC). The mechanism of this high avidity of hypericin to PS and PE may be because both PS and PE were exposed to the ^{64}Cu-labelled hypericin in the inner leaflet of damaged cell membrane in necrosis.

The above-described reports of hypericin selectively binding to cholesterol or the phospholipid targets PS and PE remain to be verified [67]]. As hypericin has various subcellular distributions—including plasma membrane, endoplasmic reticulum (ER), mitochondria, lysosome, and Golgi apparatus [68, 69]]—the observed selectivity of hypericin for cholesterol [65] or PS and PE [66, 67] might only occur because these molecules are the first to be encountered as hypericin enters cells. It is also possible that, due to the high permeability of capillaries in tumor tissue and tumor cell membranes, PS and PE in the internal leaflet of the tumor cell membrane may be exposed to some extent, like necrotic cells. This could partly explain the observations in some studies that NACAs can selectively accumulate in both necrotic tissue and viable tumors [43, 44].

Compound-specific necrosis avidity of NACAs

For some NACA molecules, it has been found that a slight modification or even an isomer transformation can eliminate necrosis targeting [45]. This suggests that the retention of hypericin in necrotic tissue and the local interaction between hypericin and necrotic debris is strictly dependent on chemical structure rather than on a simple mode of trapping or sluggish wash-in and wash-out. In other words, there is likely a compound-specific mechanism behind the necrosis targeting of different NACAs, including hypericin as evidenced from the following findings.

In recent years, tumor necrosis therapy (TNT) has emerged as a unique method of treatment. The basic principle of TNT is that targeting molecules, e.g., antigen-specific monoclonal antibodies (MAb), can carry a tumoricidal substance like ^{131}I, and be retained within the tumor tissue, resulting in tumor-specific killing. Target specificity is thus a key element of this technique. The first designated TNT was the MAb TNT-1, which was directed against nucleosomal determinants consisting of histone H1 and DNA; in contrast, other TNTs (e.g., TNT-3 and chimeric TNT) are directed against single-stranded DNA [70-73]. Duramycin is a 2-kDa small protein produced by *Streptoverticillium cinnamoneus*. Its radiolabeled derivative, ^{99m}Tc-HYNIC-duramycin, has been successfully applied in myocardial infarction imaging in a rat model of ischemia-reperfusion [74]. Duramycin reportedly targets PE, which is a main lipid component in the phospholipid bilayer structure and is exposed to duramycin after cell death [67]. Radiolabeled antimyosin MAb (^{99m}Tc-antimyosin or ^{111}In-antimyosin) reportedly has selective affinity for the heavy chain of intracellular myosin, because it is exposed after necrotic cell death. Thus, radiolabeled antimyosin can be used as a marker for imaging myocardial infarction [75-77]. These facts support the hypothesis of a compound-specific mechanism behind the necrosis affinity of NACAs, including hypericin.

Conclusions

In conclusion, hypericin has been widely studied for use as a photosensitizer in photodynamic therapy for many clinical purposes. More recently, it has been found to also have a specific avidity for necrotic tissues. This avidity is also observed in a series of radiolabeled hypericin derivatives, including [^{123}I]iodohypericin, [^{124}I]iodohypericin, and [^{131}I]iodohypericin. Therefore, hypericin has also been investigated for use as a type of NACA for noninvasively targeting necrotic tissues in numerous disorders. The potential clinical theranostic applications of hypericin include identification of acute myocardial infarction, evaluation of tissue viability, assessment of therapeutic responses to treatment, and interventional procedures for treating solid tumors [56, 78]. The mechanisms behind the necrosis avidity of hypericin and other NACAs remain to be fully elucidated, although several hypotheses have been suggested to explain the phenomenon. In particular, it has been proposed that the necrosis avidity of hypericin is compound-specific; for instance, cholesterol, PS, or PE components in the phospholipid bilayer may be the major targets of its observed selectivity. Further investigations are needed to identify the specific binding moiety that is responsible for the necrosis avidity of hypericin.

Competing Interests

The authors have declared that no competing interest exists.

References

1. Kacerovska D, Pizinger K, Majer F, et al. Photodynamic therapy of nonmelanoma skin cancer with topical hypericum perforatum extract--a pilot study. Photochem Photobiol 2008; 84:779-785.
2. Miskovsky P. Hypericin--a new antiviral and antitumor photosensitizer: mechanism of action and interaction with biological macromolecules. Curr Drug Targets 2002; 3:55-84.
3. Saw CL, Olivo M, Soo KC, et al. Spectroscopic characterization and photobleaching kinetics of hypericin-N-methyl pyrrolidone formulations. Photochem Photobiol Sci 2006; 5:1018-1023.
4. Olivo M, Lau W, Manivasager V, et al. Novel photodynamic diagnosis of bladder cancer: ex vivo fluorescence cytology using hypericin. Int J Oncol 2003; 23:1501-1504.
5. Olivo M, Du HY, Bay BH. Hypericin lights up the way for the potential treatment of nasopharyngeal cancer by photodynamic therapy. Curr Clin Pharmacol 2006; 1:217-222.
6. Rook AH, Wood GS, Duvic M, et al. A phase II placebo-controlled study of photodynamic therapy with topical hypericin and visible light irradiation in the treatment of cutaneous T-cell lymphoma and psoriasis. J Am Acad Dermatol 2010; 63:984-990.
7. Lavie G, Mazur Y, Lavie D, et al. Hypericin as an inactivator of infectious viruses in blood components. Transfusion 1995; 35:392-400.
8. Cecchini C, Cresci A, Coman MM, et al. Antimicrobial activity of seven hypericum entities from central Italy. Planta Med 2007; 73:564-566.
9. Lopez-Chicon P, Paz-Cristobal MP, Rezusta A, et al. On the mechanism of Candida spp. photoinactivation by hypericin. Photochem Photobiol Sci 2012; 11:1099-1107.
10. Ni Y, Bormans G, Chen F, et al. Necrosis avid contrast agents: functional similarity versus structural diversity. Invest Radiol 2005; 40:526-535.
11. Van de Putte M, Wang H, Chen F, et al. Hypericin as a marker for determination of tissue viability after radiofrequency ablation in a murine liver tumor model. Oncol Rep 2008; 19:927-932.
12. Van de Putte M, Ni Y, De Witte PA. Exploration of the mechanism underlying the tumor necrosis avidity of hypericin. Oncol Rep 2008; 19:921-926.
13. Van de Putte M, Wang H, Chen F, et al. Hypericin as a marker for determination of tissue viability after intratumoral ethanol injection in a murine liver tumor model. Acad Radiol 2008; 15:107-113.
14. Wang H, Miranda Cona M, Chen F, et al. Comparison between nonspecific and necrosis-avid gadolinium contrast agents in vascular disrupting agent-induced necrosis of rodent tumors at 3.0T. Invest Radiol 2011; 46:531-538.
15. Chopra A. Mono-[123I]iodohypericine monocarboxylic acid. 2004;.
16. Jin J, Teng G, Feng Y, et al. Magnetic resonance imaging of acute reperfused myocardial infarction: intraindividual comparison of ECIII-60 and Gd-DTPA in a swine model. Cardiovasc Intervent Radiol 2007; 30:248-256.
17. Ni Y, Chen F, Marchal G. Differentiation of residual tumor from benign periablational tissues after radiofrequency ablation: the role of MR imaging contrast agents. Radiology 2005; 237:745-747.
18. Ni Y, Cresens E, Adriaens P, et al. Exploring multifunctional features of necrosis avid contrast agents. Acad Radiol 2002; 9 Suppl 2:S488-490.
19. Fonge H, Jin L, Wang H, et al. Synthesis and preliminary evaluation of mono-[123I]iodohypericin monocarboxylic acid as a necrosis avid imaging agent. Bioorg Med Chem Lett 2007; 17:4001-4005.
20. Ni Y, Huyghe D, Verbeke K, et al. First preclinical evaluation of mono-[123I]iodohypericin as a necrosis-avid tracer agent. Eur J Nucl Med Mol Imaging 2006; 33:595-601.
21. Fonge H, Vunckx K, Wang H, et al. Non-invasive detection and quantification of acute myocardial infarction in rabbits using mono-[123I]iodohypericin microSPECT. Eur Heart J 2008; 29:260-269.
22. Fonge H, Van de Putte M, Huyghe D, et al. Evaluation of tumor affinity of mono-[(123)I]iodohypericin and mono-[(123)I]iodoprotohypericin in a mouse model with a RIF-1 tumor. Contrast Media Mol Imaging 2007; 2:113-119.
23. Marysael T, Bauwens M, Ni Y, et al. Pretargeting of necrotic tumors with biotinylated hypericin using (123)I-labeled avidin: evaluation of a two-step strategy. Invest New Drugs. 2011.
24. Van de Putte M, Marysael T, Fonge H, et al. Radiolabeled iodohypericin as tumor necrosis avid tracer: diagnostic and therapeutic potential. Int J Cancer 2012; 131:E129-137.
25. Li J, Sun Z, Zhang J, et al. A dual-targeting anticancer approach: soil and seed principle. Radiology 2011; 260:799-807.
26. Ni Y, Chen F, Mulier S, et al. Magnetic resonance imaging after radiofrequency ablation in a rodent model of liver tumor: tissue characterization using a novel necrosis-avid contrast agent. Eur Radiol 2006; 16:1031-1040.
27. Koljenovic S, Choo-Smith LP, Bakker Schut TC, et al. Discriminating vital tumor from necrotic tissue in human glioblastoma tissue samples by Raman spectroscopy. Lab Invest 2002; 82:1265-1277.
28. Ni Y, Marchal G, Herijgers P, et al. Paramagnetic metalloporphyrins: from enhancers of malignant tumors to markers of myocardial infarcts. Acad Radiol 1996; 3 Suppl 2:S395-397.
29. Ni Y, Marchal G, van Damme B, et al. Magnetic resonance imaging, microangiography, and histology in a rat model of primary liver cancer. Invest Radiol 1992; 27:689-697.
30. Ni Y, Marchal G, Yu J, et al. Localization of metalloporphyrin-induced "specific" enhancement in experimental liver tumors: comparison of magnetic resonance imaging, microangiographic, and histologic findings. Acad Radiol 1995; 2:687-699.
31. Ni Y, Petre C, Miao Y, et al. Magnetic resonance imaging-histomorphologic correlation studies on paramagnetic metalloporphyrins in rat models of necrosis. Invest Radiol 1997; 32:770-779.
32. Metz S, Daldrup-Unk HE, Richter T, et al. Detection and quantification of breast tumor necrosis with MR imaging: value of the necrosis-avid contrast agent Gadophrin-3. Acad Radiol 2003; 10:484-490.
33. Marchal G, Ni Y, Herijgers P, et al. Paramagnetic metalloporphyrins: infarct avid contrast agents for diagnosis of acute myocardial infarction by MRI. Eur Radiol 1996; 6:2-8.
34. Bockhorst K, Els T, Hoehn-Berlage M. Selective enhancement of experimental rat brain tumors with Gd-TPPS. J Magn Reson Imaging 1994; 4:451-456.
35. Pass HI. Photodynamic therapy in oncology: mechanisms and clinical use. J Natl Cancer Inst 1993; 85:443-456.
36. Ogan MD, Revel D, Brasch RC. Metalloporphyrin contrast enhancement of tumors in magnetic resonance imaging. A study of human carcinoma, lymphoma, and fibrosarcoma in mice. Invest Radiol 1987; 22:822-828.
37. Zhang Y, Lovell JF. Porphyrins as theranostic agents from prehistoric to modern times. Theranostics 2012; 2:905-915.
38. Ni Y, Adzamli K, Miao Y, et al. MRI contrast enhancement of necrosis by MP-2269 and gadophrin-2 in a rat model of liver infarction. Invest Radiol 2001; 36:97-103.
39. Takehara Y, Sakahara H, Masunaga H, et al. Tumour enhancement with newly developed Mn-metalloporphyrin (HOP-9P) in magnetic resonance imaging of mice. Br J Cancer 2001; 84:1681-1685.
40. Huang LR, Straubinger RM, Kahl SB, et al. Boronated metalloporphyrins: a novel approach to the diagnosis and treatment of cancer using contrast-enhanced MR imaging and neutron capture therapy. J Magn Reson Imaging 1993; 3:351-356.
41. Hindre F, Le Plouzennec M, de Certaines JD, et al. Tetra-p-aminophenylporphyrin conjugated with Gd-DTPA: tumor-specific contrast agent for MR imaging. J Magn Reson Imaging 1993; 3:59-65.
42. Noell S, Mayer D, Strauss WS, et al. Selective enrichment of hypericin in malignant glioma: pioneering in vivo results. Int J Oncol 2011; 38:1343-1348.
43. Hambright P, Fawwaz R, Valk P, et al. The distribution of various water soluble radioactive metalloporphyrins in tumor bearing mice. Bioinorg Chem 1975; 5:87-92.
44. Kim TK, Choi BI, Park SW, et al. Gadolinium mesoporphyrin as an MR imaging contrast agent in the evaluation of tumors: an experimental model of VX2 carcinoma in rabbits. AJR Am J Roentgenol 2000; 175:227-234.
45. Ni Y, Miao Y, Semmler W, et al. Manganese-metalloporphyrin (ATN-10) as a tumor-localizing agent: magnetic resonance imaging and inductively coupled plasma atomic emission spectroscopy study with experimental brain tumors. Neurosurgery 1999; 44:1146-1150.
46. Yamamoto T, Matsumura A, Shibata Y, et al. Manganese-metalloporphyrin (ATN-10) as a tumor-localizing agent: magnetic resonance imaging and inductively coupled plasma atomic emission spectroscopy study with experimental brain tumors. Neurosurgery. 1998; 42:1332-1337.
47. Saeed M, Bremerich J, Wendland MF, et al. Reperfused myocardial infarction as seen with use of necrosis-specific versus standard extracellular MR contrast media in rats. Radiology 1999; 213:247-257.

48. Maurer J, Strauss A, Ebert W, et al. Contrast-enhanced high resolution magnetic resonance imaging of pigmented malignant melanoma using Mn-TPPS4 and Gd-DTPA: experimental results. Melanoma Res 2000; 10:40-46.
49. Choi SI, Choi SH, Kim ST, et al. Irreversibly damaged myocardium at MR imaging with a necrotic tissue-specific contrast agent in a cat model. Radiology 2000; 215:863-868.
50. [Internet] http://www.magnetic-resonance.org/MagRes%20Chapters/13_03.htm.
51. Manrique A, Marie PY. [The best of nuclear cardiology and MRI in 2002]. Arch Mal Coeur Vaiss 2003; 96:73-85.
52. Daldrup-Link HE, Rudelius M, Metz S, et al. Cell tracking with gadophrin-2: a bifunctional contrast agent for MR imaging, optical imaging, and fluorescence microscopy. Eur J Nucl Med Mol Imaging 2004; 31:1312-1321.
53. Krombach GA, Higgins CB, Gunther RW, et al. [MR contrast media for cardiovascular imaging]. Rofo 2002; 174:819-829.
54. Miller DL, Li P, Dou C, et al. Evans blue staining of cardiomyocytes induced by myocardial contrast echocardiography in rats: evidence for necrosis instead of apoptosis. Ultrasound Med Biol 2007; 33:1988-1996.
55. Chen F, Suzuki Y, Nagai N, et al. Visualization of stroke with clinical MR imagers in rats: a feasibility study. Radiology 2004; 233:905-911.
56. Li J, Cona MM, Chen F, et al. Sequential systemic administrations of combretastatin A4 Phosphate and radioiodinated hypericin exert synergistic targeted theranostic effects with prolonged survival on SCID mice carrying bifocal tumor xenografts. Theranostics 2013; 3:127-137.
57. De Saint-Hubert M, Prinsen K, Mortelmans L, et al. Molecular imaging of cell death. Methods 2009; 48:178-187.
58. Ni Y. Metalloporphyrins and Functional Analogues as MRI Contrast Agents. Current Medical Imaging Reviews 2008;:96-112.
59. Hofmann B, Bogdanov A, Jr., Marecos E, et al. Mechanism of gadophrin-2 accumulation in tumor necrosis. J Magn Reson Imaging 1999; 9:336-341.
60. Van de Putte M, Roskams T, Vandenheede JR, et al. Elucidation of the tumoritropic principle of hypericin. Br J Cancer 2005; 92:1406-1413.
61. Mukherjee P, Adhikary R, Halder M, et al. Accumulation and interaction of hypericin in low-density lipoprotein--a photophysical study. Photochem Photobiol 2008; 84:706-712.
62. Buriankova L, Buzova D, Chorvat D, Jr., et al. Kinetics of hypericin association with low-density lipoproteins. Photochem Photobiol 2011; 87:56-63.
63. Kascakova S, Nadova Z, Mateasik A, et al. High level of low-density lipoprotein receptors enhance hypericin uptake by U-87 MG cells in the presence of LDL. Photochem Photobiol 2008; 84:120-127.
64. English DS, Doyle RT, Petrich JW, et al. Subcellular distributions and excited-state processes of hypericin in neurons. Photochem Photobiol 1999; 69:301-305.
65. Ho YF, Wu MH, Cheng BH, et al. Lipid-mediated preferential localization of hypericin in lipid membranes. Biochim Biophys Acta 2009; 1788:1287-1295.
66. Song S, Xiong C, Zhou M, et al. Small-animal PET of tumor damage induced by photothermal ablation with 64Cu-bis-DOTA-hypericin. J Nucl Med 2011; 52:792-799.
67. Belhocine TZ, Prato FS. Transbilayer phospholipids molecular imaging. EJNMMI Res 2011; 1:17.
68. Agostinis P, Vantieghem A, Merlevede W, et al. Hypericin in cancer treatment: more light on the way. Int J Biochem Cell Biol 2002; 34:221-241.
69. Ali SM, Olivo M. Bio-distribution and subcellular localization of Hypericin and its role in PDT induced apoptosis in cancer cells. Int J Oncol 2002; 21:531-540.
70. Hornick JL, Sharifi J, Khawli LA, et al. A new chemically modified chimeric TNT-3 monoclonal antibody directed against DNA for the radioimmunotherapy of solid tumors. Cancer Biother Radiopharm 1998; 13:255-268.
71. Chen S, Yu L, Jiang C, et al. Pivotal study of iodine-131-labeled chimeric tumor necrosis treatment radioimmunotherapy in patients with advanced lung cancer. J Clin Oncol 2005; 23:1538-1547.
72. Street HH, Goris ML, Fisher GA, et al. Phase I study of 131I-chimeric(ch) TNT-1/B monoclonal antibody for the treatment of advanced colon cancer. Cancer Biother Radiopharm 2006; 21:243-256.
73. Khawli LA, Mizokami MM, Sharifi J, et al. Pharmacokinetic characteristics and biodistribution of radioiodinated chimeric TNT-1, -2, and -3 monoclonal antibodies after chemical modification with biotin. Cancer Biother Radiopharm 2002; 17:359-370.
74. Zhao M, Li Z, Bugenhagen S. 99mTc-labeled duramycin as a novel phosphatidylethanolamine-binding molecular probe. J Nucl Med 2008; 49:1345-1352.
75. Khaw BA, Gold HK, Yasuda T, et al. Scintigraphic quantification of myocardial necrosis in patients after intravenous injection of myosin-specific antibody. Circulation 1986; 74:501-508.
76. Keyes JW, Leonard PF, Brody SL, et al. Myocardial infarct quantification in the dog by single photon emission computed tomography. Circulation 1978; 58:227-232.
77. Flotats A, Carrio I. Non-invasive in vivo imaging of myocardial apoptosis and necrosis. Eur J Nucl Med Mol Imaging 2003; 30:615-630.
78. Li J, Cona MM, Chen F, et al. Exploring theranostic potentials of radioiodinated hypericin in rodent necrosis models. Theranostics 2012; 2:1010-1019.